Evaluation of HOCl-generating anticancer agents by an ultrasensitive dual-mode fluorescent probe

Blue-to-red "fluorescence rainbow" probes C1-C7 were developed and shown to sensitively and rapidly detect HOCl in the biologically relevant concentration range with fluorescence turn-on observed in their respective optical regions, providing a broad selection of colors for imaging HOCl *in vivo*. Remarkably, C7, a dual-mode fluorescent probe for both low and high concentrations of HOCl, could be used to monitor the oxidative stress process induced by elesclomol in live cancer cells, and using C7 it was further discovered that an evodiamine derivative was capable of generating cancer-cell HOCl.

As featured in:
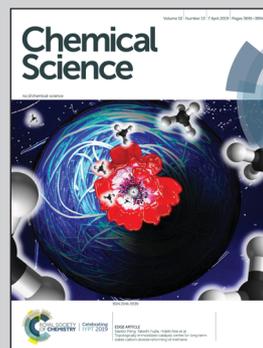
ROYAL SOCIETY OF CHEMISTRY | Celebrating IYPT 2019

rsc.li/chemical-science

Check for updates

Evaluation of HOCl-generating anticancer agents by an ultrasensitive dual-mode fluorescent probe†

Donglei Shi,‡[a] Shuqiang Chen,‡[b] Biao Dong, [iD] ‡[c] Yanhui Zhang,[a] Chunquan Sheng, [iD] [b] Tony D. James [iD] [d] and Yuan Guo [iD] *[a]

Hypochlorous acid (HOCl), a reactive oxygen species (ROS), plays a crucial role in the process of pathogenic oxidative stress. Some powerful anticancer agents, such as elesclomol, specifically induce cancer cell apoptosis by increasing HOCl levels. However, sensitive tools to monitor subtle changes of biological HOCl *in vivo* are limited. To achieve this, we herein present rationally designed probes **C1–C7** through introducing a bioorthogonal dimethylthiocarbamate receptor. All the probes were shown to sensitively and rapidly detect HOCl in the nanomolar/biologically relevant concentration range with fluorescence turn-on observed in their respective optical regions, resulting in a blue-to-red "fluorescence rainbow" and providing a broad selection of colors for imaging HOCl *in vivo*. Remarkably, probe **C7** exhibited both a turn-on signal at biologically relevant concentrations (LOD_1 = 18 nM) and a ratiometric response at the high risk pathogenic concentrations (LOD_2 = 0.47 μM), which gives a higher reliability compared to a single signal and avoids cross-talk caused by the combined use of several probes. **C7** was used to monitor the oxidative stress process induced by elesclomol in live cancer cells, and using this probe it was further discovered that an evodiamine derivative was capable of generating cancer-cell HOCl.

Introduction

Reactive oxygen species (ROS) are a hallmark of various pathophysiological processes and have close links with many diseases including cancer, aging, inflammation and neuro-degenerative disorders.[1–8] They have recently gained enormous attention especially in preclinical medicine and life sciences.[9–13] ROS are formed as a normal by-product of aerobic metabolism and are indispensable for cell signaling and immune response, but can be generated in excess under pathophysiological conditions.[14] Although the generation of excessive ROS leads to diseases related with oxidative stress damage, some anticancer agents such as elesclomol (a potential drug candidate) specifically induce cancer cell

apoptosis by increasing ROS levels.[15–23] However, the lack of efficient ROS detection methods for specific concentration ranges in live systems has restricted the pace of progress in the discovery of this type of drug and a deeper understanding of the precise role of ROS in diseases.

Endogenous hypochlorous acid (HOCl) is a particularly interesting type of ROS that plays a crucial role in the oxidative stress process induced by anticancer drugs or pathogenic factors.[24] Biologically, HOCl is mainly derived from mitochondria in neutrophils and monocytes, because myeloperoxidase (MPO) living in the mitochondria is the catalyst for converting chloride ions (Cl^-) and hydrogen peroxide (H_2O_2) to HOCl.[25] Therefore, for the purpose of a pathogenesis investigation or drug discovery, real-time discrimination and quantitative analysis of biological HOCl in live systems, especially mitochondrial HOCl, is of particular interest. To this end, a number of excellent fluorescent probes for the detection and imaging of HOCl have been developed over the past few years.[26–40] However, few of them can target live-cell mitochondria, which is essential for real-time and accurate sensing. More importantly, a single fluorescent probe for sensing different concentration ranges of HOCl with distinct modes of fluorescence signals has several advantages, such as a higher reliability compared to a single signal and avoids cross-talk caused by the use of multiple probes.[41–43] Nevertheless, to date there are no small-molecule probes to achieve this purpose, resulting in imaging biological HOCl in cells only with single fluorescent signal mode (Fig. 1a).

[a]*Key Laboratory of Synthetic and Natural Functional Molecule Chemistry of the Ministry of Education, National Demonstration Center for Experimental Chemistry Education, College of Chemistry and Materials Science, Northwest University, Xi'an 710127, China. E-mail: guoyuan@nwu.edu.cn*

[b]*School of Pharmacy, Second Military Medical University, 325 Guohe Road, Shanghai 200433, China*

[c]*State Key Laboratory on Integrated Optoelectronics, College of Electronic Science and Engineering, Jilin University, Changchun 130012, China*

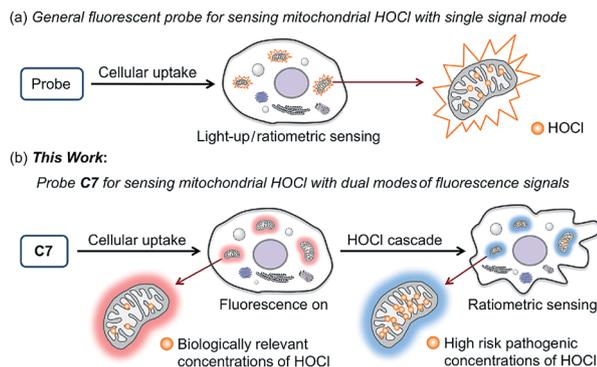[d]*Department of Chemistry, University of Bath, Bath BA2 7AY, UK*

Fig. 1 Schematic representation of mitochondrial HOCl sensed by general fluorescent probe (a) and our probe **C7** (b) in live cells.

In this work, we present seven novel fluorescent probes **C1**–**C7** for imaging HOCl *in vitro* and *in vivo*, all of which can rapidly detect a biologically relevant concentration of HOCl with fluorescence turn-on observed in their respective optical regions and spanning blue to red (453 to 630 nm), resulting in a "fluorescence rainbow". These probes proved to be highly selective to HOCl among various ROS, and produce a very sensitive fluorescence response to HOCl, thereby ensuring the specific and real-time detection of endogenous HOCl in live cells. Among them, the **C6** and **C7** can target live-cell mitochondria with high reactivity and very short half-life. Remarkably, probe **C7** can for the first time as a single molecule detect two concentration ranges of HOCl (Fig. 1b). Using **C7** in live-cell confocal imaging, we obtained a clear and exact view of the cancer cell oxidative stress process induced by elesclomol, an experimental anticancer agent based on promoting ROS,[21–23] and discovered that evodiamine derivatives have a similar anticancer mechanism. Furthermore, the red-emitting **C6** and **C7** were used for the imaging of HOCl in live *C. elegans* and mice respectively.

Results and discussion

Structurally, probes **C1**–**C7** each consist of a *N,N*-dimethylthiocarbamate group, which is an ideal entropy-driven receptor for HOCl first reported by Tang in 2016.[44] Following the seminal work, a number of groups have developed HOCl probes with this group owing to its fast and ultrasensitive response.[45–48] However, none of them constructed thiocarbamate analogues to further systematically investigate the response mechanism. To achieve this aim, we designed two additional types of candidate probe molecules (**A** and **B**) by interchanging the S atom and the O atom in the thiocarbamate moiety (Fig. 2a). The results revealed that the S atom was indispensable and could best be located on the double bond, suggesting that **C** analogs with a thiocarbamate group are the most sensitive among them (Fig. S1†). This could be reasonably explained by their entropy-driven reaction mechanism based on the release of gas molecules (Scheme S1†). Therefore, we designed and synthesized probes **C1**–**C7** by coupling the thiocarbamate group with diverse phenolic fluorophores, including coumarin (**C1**–**C3**) and 2-(2-hydroxyphenyl)benzothiazole (HBT) (**C4**–**C7**) scaffolds.
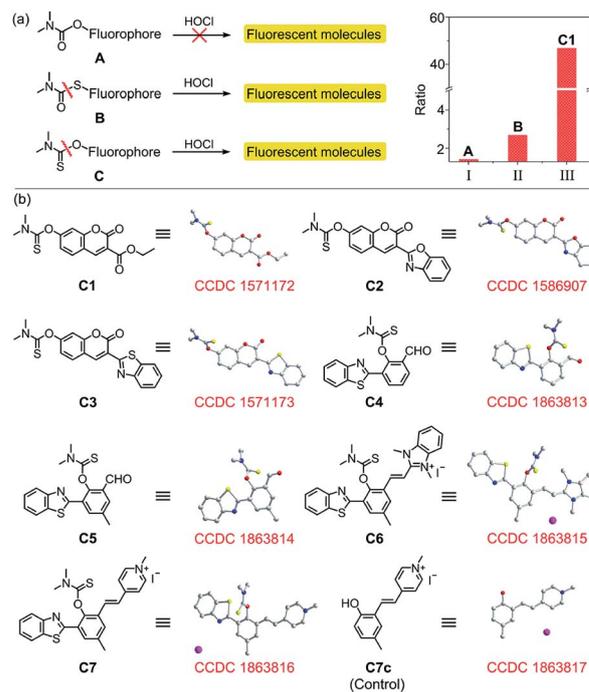

Fig. 2 (a) Response of **A**, **B** and **C** to HOCl and the fluorescence ratios of **A**, **B** and **C1**. Column I: ratio = $F_{A+4\ equiv.\ HOCl}/F_A$; column II: ratio = $F_{B+4\ equiv.\ HOCl}/F_B$; column III: ratio = $F_{C1+2\ equiv.\ HOCl}/F_{C1}$; (b) chemical structures and X-ray crystal structures of probes and control compound **C7c**.

Furthermore, considering that small molecules containing organic cations are capable of accumulating inside mitochondria under the attraction of the negative potential of the inner membrane thereof,[49–51] the mitochondria-targeting probes **C6** and **C7** were synthesized by introducing benzimidazolium and pyridinium cations as mitochondria-targeting groups, respectively. The synthetic routes of **C1**–**C7** are illustrated in Scheme S2.† All compounds were characterized by ^{1}H NMR, ^{13}C NMR and HRMS and the original spectra are included in the ESI.† Moreover, we obtained the X-ray crystal structures of compound **A** (Scheme S2†), compound **C7c** and all probes (**C1**–**C7**) (Fig. 2b) to further confirm their chemical structures.

The emission and absorption spectra of probes **C1**–**C7** before and after the addition of HOCl were recorded in an aqueous medium buffered to physiological pH (Fig. 3a, b, S2 and S3†). Upon the addition of various low concentration ranges of HOCl, the seven probes all exhibited a significant increase in fluorescence, especially **C3** which showed a 223-fold increase in fluorescence (Table S2†). All the probes have a large Stokes shift, which effectively avoids the self-absorption of the fluorescence, with **C7** possessing the largest Stokes shift (170 nm, Table 1). The plots of fluorescence intensity of **C1**–**C7** against HOCl at a low concentration all showed a good linear relationship (with a linear correlation coefficient R^2 greater than 0.99) (Fig. 3a, b and S3†). Moreover, all these probes have a low limit of detection (LOD) (0.94–23 nM, Table 1). On continued addition of HOCl, **C1**–**C6** exhibited negligible changes in their fluorescence spectra, while **C7** showed a notable 48-fold fluorescence
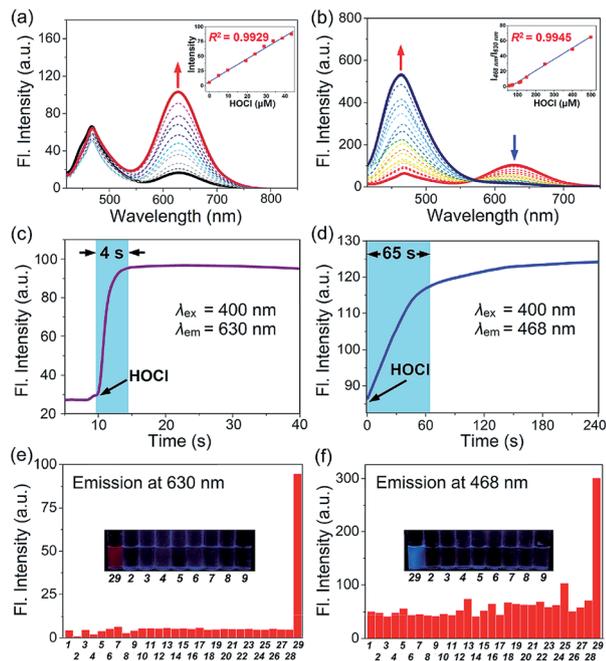
Fig. 3 (a) Fluorescence spectra of **C7** (10 μM) in HEPES solution (10 mM, pH = 7.4, MeOH : water = 1 : 4 v/v) change as a function of HOCl (at 0−60 μM). Inset: fluorescent intensity changes at 630 nm upon the addition of low concentrations of HOCl (0−60 μM); (b) fluorescence spectra of **C7** (10 μM) change as a function of HOCl (at 60−330 μM). Inset: fluorescent intensity of I_{468}/I_{630} changes upon the addition of high concentrations of HOCl (60−330 μM); (c) time course of fluorescence intensity of **C7** (10 μM) at 630 nm after the addition of 60 μM HOCl (time range 0−40 s); (d) time course of fluorescence intensity of **C7** (10 μM) at 468 nm after addition of 120 μM HOCl (time range 0−240 s); (e) fluorescent intensity of **C7** in presence of 60 μM and (f) 200 μM various ROS and relevant analytes. Inset: photographs of **C7** after the addition of HOCl (60 μM and 200 μM) under a UV lamp (365 nm). (1) Blank, (2) H_2O_2, (3) $^\bullet OH$, (4) $O_2^{\bullet -}$, (5) $^1O_2$, (6) $NO^\bullet$, (7) $TBO^\bullet$, (8) TBHP, (9) $ONOO^-$, (10) HSO_3^-, (11) F^-, (12) Cl^-, (13) SCN^-, (14) NO_2^-, (15) HSO_4^-, (16) $S_2O_3^{2-}$, (17) HPO_4^-, (18) I^-, (19) PO_4^{3-}, (20) Br^-, (21) HCO_3^-, (22) SO_4^{2-}, (23) $H_2PO_4^{2-}$, (24) CO_3^{2-}, (25) NO_3^-, (26) Hcy, (27) GSH, (28) Cys, (29) HOCl.

ratio (I_{468}/I_{630}) enhancement with a good linear relationship (R^2 = 0.9945) and a new limit of detection (0.47 μM). In good agreement, **C1–C7** all showed a remarkable red-shift in their

absorption spectra upon treatment with HOCl (Fig. S2a−g†). For probe **C7**, the continued increase in HOCl concentration generated a new absorption peak at 275 nm at the expense of decreasing the absorption peak at 330 nm (Fig. S2h†). Our results indicated that **C1–C7** all display an excellent sensitivity in detecting nanomolar/biologically relevant concentrations of HOCl with a fluorometric turn-on signal in response, whereas only **C7** exhibited a ratiometric response to micromolar/high risk pathogenic concentrations of HOCl.

Subsequently, we evaluated the reaction kinetics of **C1–C7** with HOCl (Fig. 3c, d and S4†). Upon the addition of various low concentrations of HOCl, the fluorescence intensity of all probes reached a maximum within 18 s (Table 1), indicating that the probes can rapidly respond to HOCl. Notably, the reaction of probe **C7** with HOCl was completed within 4 s. While, titration with a micromolar concentration of HOCl (120 μM) caused that time-dependent fluorescence intensity changes of **C7** was completed in *ca.* 65 s.

Next, the effect of pH changes on the probes to HOCl over a wide pH range from 3–11 was evaluated. As shown in Fig. S5,† on the addition of various low concentrations of HOCl, the fluorescence intensity of probes **C1–C7** displayed negligible changes at pH ranging from 6.0 to 7.7, while **C7** also exhibited a stable response to a micromolar concentration of HOCl over that pH range. The results indicated that our probes could be applied to detect HOCl at physiological pH. To test the selectivity of **C1–C7** for HOCl, the fluorescence response of probes **C1–C7** to diverse interfering species including metal ions (Fig. S6†), anion species and biothiols (Fig. 3e, f and S7†) was investigated. The results indicate that none of the interfering species induced any obvious fluorescence changes with any of the probes, even at concentrations as high as 200 μM. Moreover, the fluorescence response of the probes to HOCl in the presence of other interfering species was almost the same as in the absence of these species, suggesting that the presence of other species will not influence the reaction of the probes with HOCl. The results indicated that probes **C1–C7** can selectively detect HOCl over other common interfering species.

The mechanism for the reaction of **C1–C7** with HOCl in the nanomolar concentration range to release fluorophores **C1p–**

Table 1 Properties of **C1–C7**

Probes	λ_{abs}^a (nm)	λ_{em}^b (nm)	Stokes shift (nm)	Reaction time^c (s)	LOD^d (nM)
C1	405	454	49	8	6.5
C2	427	494	67	6	9.1
C3	422	502	80	8	0.94
C4	435	532	97	18	7.5
C5	440	550	110	10	2.7
C6	464	615	151	4	23
C7	460	630	170	4	18
C7^e	330	468	138	65	0.47 μM

^{a} Maximum absorption wavelength (λ_{abs}). ^{b} Maximum emission wavelength (λ_{em}) of corresponding probes. ^{c} The reaction time of our probes to HOCl. ^{d} The limit of detection of corresponding probes. ^{e} The properties of probe **C7** at micromolar level of HOCl. The optical properties of **C1** were conducted in pH 7.4 PBS buffer. The optical properties of **C2–C4** were conducted in pH 7.4 PBS buffer (10 mM) with 10% MeOH. The optical properties of **C5** were conducted in pH 7.4 PBS buffer (10 mM) with 5% EtOH. The optical properties of **C6** were conducted in pH 7.4 PBS buffer (10 mM) with 20% EtOH. The optical properties of **C7** were conducted in pH 7.4 HEPES buffer (10 mM) with 20% MeOH.

C7p was investigated on the basis of the reported literature (Scheme S1†), and can be explained by the contribution of Cl^+ from HOCl to the release of the thiocarbamate moiety which acts as a "fluorophore mask".[43] To verify this hypothesis, **C1p–C7p** were prepared (Scheme S2†) and analyzed by both fluorescence spectroscopy (Fig. S8†) and electrospray ionization (ESI) mass spectrometry (Fig. S9–S15†). As shown in Fig. S8,† the emission wavelength of **C1p–C7p** is consistent with that of the corresponding probe treated with HOCl in the nanomolar concentration range, and the reaction of each probe with HOCl generates a peak in the ESI mass spectrum which matches the peak position of the respective **C1p–C7p**. This confirmed the release of the thiocarbamate and the turn-on fluorescent responses. Probe **C7** exhibits an obvious red fluorescent turn-on response to HOCl in the nanomolar concentration range due to HOCl-specific activation of the excited state intramolecular proton transfer (ESIPT) and intramolecular charge transfer (ICT) structure (**C7p**) (Fig. 4a). The optical properties of **C7p** in various solvents including aqueous solution with different contents of CTAB were studied. As shown in Fig. S16,† the fluorescence emission of **C7p** changed in different media, confirming the environmental sensitivity of the ESIPT process. More interestingly, **C7p** can further produce a sensitive ratiometric response to HOCl at a micromolar concentration with a remarkable fluorescence blue shift from 630 to 468 nm. To clarify the second-step response mechanism of **C7**, ^{1}H NMR and mass titration for HOCl were carried out. Fig. S17 and S18†

showed that no obvious changes were observed in the spectra of the products when the concentration of HOCl in the **C7**/HOCl system was increased from nanomolar to micromolar range. Also considering that the blue fluorescence increase occurs at around the pK_a of HOCl (7.54) (Fig. S5h†), we conclude that the molecule of HOCl plays the major function by complexing with **C7-OH**. Thus, we speculated that this process was attributed to deprotonation (**C7-OH** → **C7-O⋯H-OCl** → **C7-O⁻**) of the phenol unit occurs to inhibit the ESIPT process at micromolar concentrations of HOCl (Fig. 4a). To test the feasibility of our hypothesis, we designed and prepared a control compound **C7c** with the same conjugate push–pull system as **C7-O⁻** (Fig. 4c) and obtained its crystal structure. The optical properties of **C7c** were consistent with those of **C7-O⁻** (Fig. 4b), verifying the response mechanism.

Encouraged by the optical properties of **C1–C7** to HOCl *in vitro*, we next evaluated the capability of the probes to image HOCl in live cells. On the basis of the different emission wavelengths of **C1–C7**, we selected probes **C1**, **C3–C7** for imaging exogenous HOCl in live cells. They all exhibited low cytotoxicity in live cells (Fig. S19†), which is important for biological applications. HepG2 cells and A549 cells were selected for the following experiments. Fig. 5 shows, the cells which were incubated separately with probes **C1** and **C3–C7** exhibited negligible fluorescence in their corresponding channels; however, remarkable fluorescence was observed after the addition of a low concentration of HOCl. As expected, with the increase in the concentration of HOCl, the fluorescence intensity of cells treated respectively with **C1** and **C3–C6** gradually increased (Fig. S20–S24†), while cells incubated with **C7** showed an enhanced fluorescence in the red channel upon the addition of a low concentration of HOCl and then exhibited a gradual increase in the fluorescence of the blue channel and a gradually reduced fluorescence in the red channel after the addition of micromolar concentrations of HOCl (Fig. S25†). These results indicate that probes (**C1**, **C3–C7**) have excellent cell permeability
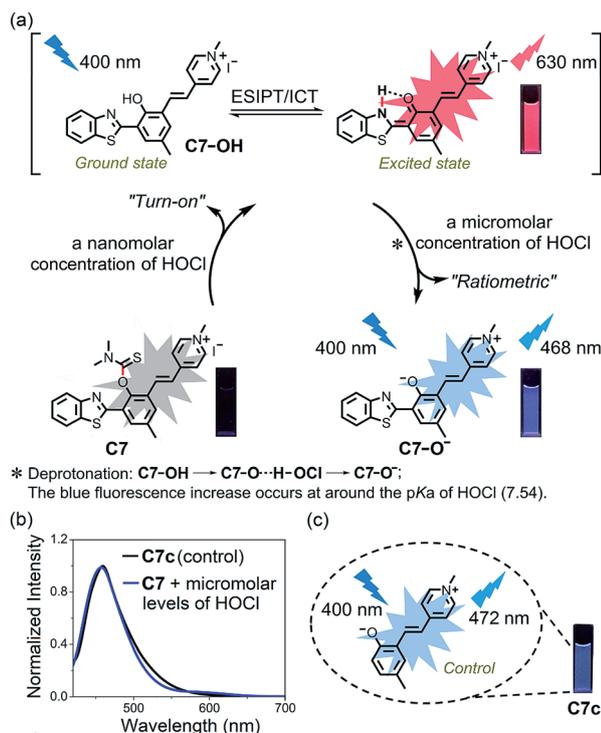

Fig. 4 (a) Proposed detection mechanism of **C7** for distinct concentration ranges of HOCl. The photographs were taken under illumination with a UV lamp (365 nm); (b) normalized fluorescence spectra of **C7c** and **C7** with addition of micromolar concentrations of HOCl (330 μM); (c) the photograph of **C7c** illuminated by a UV lamp (365 nm).
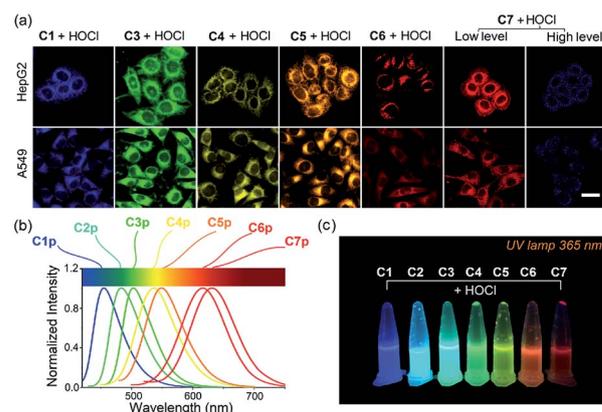

Fig. 5 (a) Confocal fluorescence images of HepG2 and A549 cells preloaded on **C1**, **C3–C7** (10 μM, 10 min) and further incubated in buffers with various concentrations of HOCl. Scale bar: 20 μm; (b) normalized fluorescence spectra of **C1p–C7p**; (c) photographs of probes **C1–C7** with the addition of HOCl were taken under illumination with a UV lamp.

to live cells and were able to visualize exogenous HOCl by fluorescence, thus offering a good range of choices for imaging HOCl in live cells. To our delight, **C7** displayed both a turn-on signal to a low concentration of HOCl and a ratiometric response to a high concentration of HOCl in live cells. Next, the potential for probes **C6** and **C7** to detect endogenous HOCl in live cells was evaluated. Bacterial endotoxin lipopolysaccharide (LPS) is known to induce cellular apoptosis and release ROS, including HOCl.[32–34] HepG2 cells and A549 cells were pretreated with LPS for three hours, and the stimulated cells were then incubated with **C6** and **C7** (20 μM), respectively. As shown in Fig. S26 and S27,† there was almost no fluorescence in the control group without treatment by LPS, suggesting that the observed changes in fluorescence intensity of the stimulated cells could be attributed to the generation of HOCl induced by LPS. Conversely, 4-aminobenzoic hydrazide (ABH), a specific MPO inhibitor, can decrease the concentration of biological HOCl in cells.[36–38] As expected, the introduction of ABH caused an obviously decreased fluorescence in the red channel (Fig S27†), further confirming the specific response of **C7** to HOCl. Thus, these data demonstrated that our probes could sensitively detect both exogenous and endogenous HOCl in live cells.

To confirm the mitochondria-targeting capacity of **C6** and **C7**, probes and different commercial staining dyes (MitoTracker Green FM, LysoTracker Green DND-26 and Golgi Tracker Green (NBD C6-ceramide)) were separately coincubated in live HeGp2 cells and then treated with HOCl for another 1 minute. Fig. 6 and S28† indicate that the fluorescence in the red channel of probe **C6** or **C7** treated with HOCl almost completely overlaps the fluorescence of MitoTracker Green in the green channel. The Pearson's correlation coefficients (PCC) of **C6** and **C7** were 0.95 and 0.90, respectively. In comparison, the fluorescence in the red channel of probes treated with HOCl partly overlaps that of LysoTracker or Golgi Tracker, with PCC values below 0.6. The correlation mapping of the fluorescence intensity also exhibited
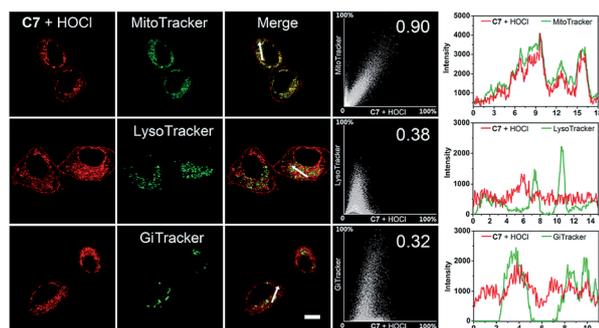
excellent colocalization between the probes and MitoTracker Green. The results indicate that **C6** and **C7** have an excellent targeting ability and are capable of monitoring mitochondrial HOCl in live cells.

Elesclomol is a known ROS-generating anticancer agent. In 2014, the group of Peng demonstrated for the first time that elesclomol can elevate HOCl levels beyond a threshold, which ultimately triggers apoptosis of cancer cells.[24] Therefore, we used elesclomol to assess the feasibility of using **C7** to monitor the fluctuation in concentration of intracellular HOCl (Fig. 7b). According to the common method of pharmacochemistry, HepG2 cell samples were treated with elesclomol (0.8 μM) for different times. The elesclomol-stimulated cells were stained with both **C7** and MitoTracker Green for 30 min and then imaged by confocal fluorescence microscopy immediately. As shown in Fig. 7a, control cells treated with **C7** only displayed negligible fluorescence in the red channel (610–650 nm) and no fluorescence in the blue channel (440–490 nm). When the incubation times of elesclomol were extended from 0 to 6 h, the fluorescence intensity of the red channel gradually enhanced, while there were no changes in the blue channel. However, there was a dramatic fluorescence enhancement of the blue channel and a decreased fluorescence of the red channel when the incubation time was prolonged from 6 h to 24 h. The time-dependent color changes can be observed quite clearly in the merged images. The results above suggested that the concentration of HOCl in elesclomol-stimulated cells increased over time and reached the high risk pathogenic level after 6 hours and confirmed that the concentration of HOCl indeed increased in the apoptosis process of cancer cell induced by the drug.

We then investigated if the probe could be applied to evaluate the underlying mechanism responsible for the action of anticancer molecules isolated from natural products. Within our research group, we have been particularly interested in developing evodiamine-based anticancer drugs/molecules. Among the novel evodiamine derivatives bearing various substitutions or a modified scaffold that we have synthesized, 3-fluoro-10-hydroxy evodiamine (**HF-EVO**) was screened and has been proven as a powerful anticancer molecule (Fig. 7c).[52] However, the underlying mechanism of **HF-EVO** responsible for the proapoptotic activity has not been elucidated in detail. We therefore employed **C7** to monitor the level of HOCl in the **HF-EVO**-induced cancer cell apoptosis process to determine whether **HF-EVO** has the same anticancer mechanism as elesclomol. For this purpose, the HepG2 cells were treated with the **HF-EVO** (0.4 μM) for different times, then incubated with **C7** and imaged by fluorescence microscopy. As expected, fluorescence changes were observed in **HF-EVO**-stimulated cells after incubation with **C7**. As depicted in Fig. 7d, control cells treated with **C7** alone exhibited fairly weak fluorescence in the red channel (610–650 nm) and no fluorescence in the blue channel (440–490 nm), while a bright fluorescence in the red channel was observed upon stimulation by **HF-EVO** for 6 hours. Then, with prolonging incubation time (6–24 h), the fluorescence intensity of HepG2 cells stimulated by **HF-EVO** and probe exhibited a clear time-dependent decrease in the red channel (Fig. 7e), accompanied by a gradual time-dependent

Fig. 6 Intracellular localization of **C7** in HepG2 cells. Fluorescence imaging of HepG2 cells incubated with 20 μM **C7**, and then stained with MitoTracker Green FM (200 nM), LysoTracker Green DND-26 (7.5 nM) and Golgi Tracker Green (NBD C6-ceramide, 3 μM), respectively. Cells were incubated with dyes and then treated with HOCl before confocal imaging. Plots in the column 4 represent the intensity correlation plot of dyes and probes. Column 5 represents cross-sectional analysis along the white line in the insets. Red channel: $\lambda_{ex} = 405$ nm, $\lambda_{em} = 610$–650 nm; green channel: $\lambda_{ex} = 488$ nm, $\lambda_{em} = 490$–550 nm. Scale bar: 10 μm.
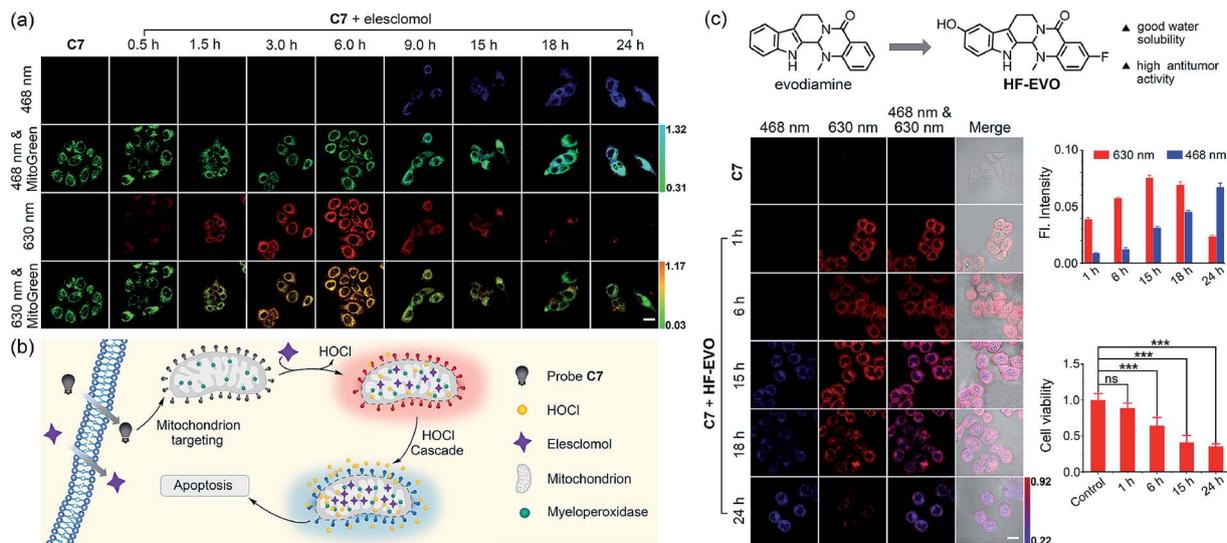
Fig. 7 (a) Time-dependent HOCl generation induced by elesclomol in live HepG2 cells. Cells were stimulated by elesclomol for different time intervals (0 h, 0.5 h, 1.5 h, 3.0 h, 6.0 h, 9.0 h, 15 h, 18 h and 24 h), and the elesclomol-stimulated cells were imaged by confocal fluorescence microscopy after staining with probe **C7** (20 μM) and MitoTracker Green (200 nM). Ratio = $F_{440-490 \text{ nm}}/F_{490-530 \text{ nm}}$ and $F_{610-650 \text{ nm}}/F_{490-530 \text{ nm}}$; (b) schematic illustration of mitochondrial HOCl monitored by probe **C7** in elesclomol-stimulated cells; (c) the structures of evodiamine and **HF-EVO** (top); time-dependent HOCl generation induced by **HF-EVO** in live HepG2 cells (left, bottom). Cells were stimulated by **HF-EVO** for different times intervals (1 h, 6 h, 15 h, 18 h, 24 h), and then the cells were imaged by confocal fluorescence microscopy after staining with probe **C7** (20 μM). Ratio = $F_{610-650 \text{ nm}}/F_{440-490 \text{ nm}}$; quantified relative fluorescent intensity in red channel and blue channel of cells (right, middle); cell viability after incubation of **HF-EVO** for different time intervals with HepG2 cells (right, bottom). The values are the mean ± s.d. for $n = 3$, ***$p < 0.001$. ns = not significant. Blue channel: $\lambda_{ex} = 405$ nm, $\lambda_{em} = 440-490$ nm; green channel: $\lambda_{ex} = 488$ nm, $\lambda_{em} = 490-530$ nm; red channel: $\lambda_{ex} = 405$ nm, $\lambda_{em} = 610-650$ nm. Scale bars: 20 μm (a, d).

fluorescence intensity increase in the blue channel. These results demonstrated that **HF-EVO** gradually increased the HOCl content over time in HepG2 cells and that the concentration of HOCl reached the high risk pathogenic level after 6 hours. Moreover, to evaluate the capacity of **HF-EVO** to induce HepG2 cell apoptosis, the cytotoxicity of **HF-EVO** against HepG2 cells was evaluated by CCK8 assay at different time periods. Fig. 7f shows, upon incubation for four different time intervals, a significant increase in the percentage of apoptotic cells was observed over time, suggesting that **HF-EVO** has a high proapoptotic activity in HepG2 cells. The results revealed that **HF-EVO** induced the accumulation of HOCl in HepG2 cells to trigger apoptosis. Taken together, these results point to the feasibility of our probe **C7** for evaluating HOCl-generating anticancer drugs, and provides a desirable chemical tool for investigating the mechanism of action of these drugs.

Inspired by the above results, we sought to image exogenous and endogenous HOCl in small laboratory animals. *C. elegans* were incubated with 490 μL M9 and 10 μL **C6** (10 μM) at 20 °C for 2 hours in the dark. Different amounts of HOCl were added to each group and the groups incubated for another 30 min. As shown in Fig. 8a, *C. elegans* prestained with **C6** exhibited very weak fluorescence but exhibited a significant fluorescence after incubating with 3 equiv. HOCl. The fluorescence intensity of *C. elegans* was enhanced with an increasing concentration of HOCl (Fig. 8b). Moreover, the favorable attributes of **C7** encouraged us to evaluate if endogenous HOCl can be monitored in live mice. Kunming mice were divided into an experimental group and

a control group to investigate the detection ability of probe **C7** for native HOCl *in vivo*. The experimental group was given an intraperitoneal (i.p.) injection of 1 mL LPS (0.3 mg mL^{-1}) and bred for 12 hours, while the control group was given an intraperitoneal (i.p.) injection of 1 mL saline. After 12 hours, a solution of **C7** (30 μM, in 0.2 mL DMSO) was injected into the abdomen of the mice for 5 minutes and then the mice subsequently anesthetized and imaged by an IVIS Spectrum small animal *in vivo* imaging system. All animal experiments were approved by the Ethics Committee of Northwest University, and were conducted in accordance with European guidelines for the care and use of laboratory animals. As shown in Fig. 8d, the experimental group stimulated with LPS displayed a much higher fluorescence readout (pseudo-color) than the control group in the red channel. A plot of fluorescence intensity measured at the abdomen of the two groups against time is shown in Fig. 8e. The fluorescence intensity of the experimental group gradually increased and displayed the strongest fluorescence at 10 min. Interestingly, the control group also exhibited a slight fluorescence enhancement, suggesting that **C7** was sensitive enough to monitor native HOCl in live mice without external stimulation. These results indicate that our probes could detect exogenous and endogenous HOCl in live animals.

Conclusions

In summary, we have designed and prepared three types of potential HOCl fluorescent probes (**A**, **B** and **C**) that were
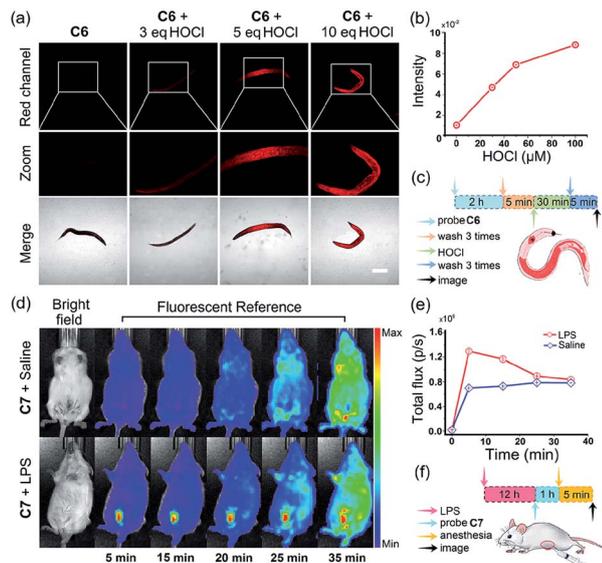
Fig. 8 (a) Confocal fluorescence images of *C. elegans* preloaded on **C6** (10 μM, 2 h) and further incubated in buffers with various concentrations of HOCl (10 μM, 50 μM, 100 μM) (λ_{ex} = 488 nm, λ_{em} = 595–635 nm. Scale bar = 200 μm); (b) quantified relative fluorescence intensity of images of *C. elegans*; (c) schematic illustration of the fluorescence images of exogenous HOCl in *C. elegans*; (d) fluorescent imaging of a Kun-ming mouse given an i.p. of LPS (0.3 mg) and bred for 12 hours; another Kun-ming mouse was given an i.p. of saline and bred for 12 hours as a control group. Images were taken after giving an i.p. of **C7** (30 μM), respectively. Images were taken using an excitation laser at 430 nm and a 620 nm emission filter; (e) fluorescence intensities of Kun-ming mouse in two group; (f) schematic illustration of the fluorescence images of endogenous HOCl in mice.

evaluated through their fluorescence response to HOCl under physiological conditions. Initial screening enabled us to delineate the structural determinants for selective recognition of HOCl. The follow-up studies demonstrated that the biocompatible thiocarbamate-based probes **C1–C7** with high sensitivity and selectivity are desirable. The various fluorescent dyes emitted over a spectral region spanning blue to red and thus provide a wide range of choices for imaging HOCl *in vivo*. In particular, the ESIPT and ICT probe **C7** can target mitochondria and display different fluorescence responses to both low and high concentrations of HOCl: an obvious turn-on signal to nanomolar concentrations of HOCl (biologically relevant concentrations, LOD_1 = 18 nM) and a subsequent ratiometric response to HOCl at the micromolar level (high risk pathogenic concentrations, LOD_2 = 0.47 μM) were observed. Better still, we achieved the distinct visualization of elesclomol-induced biological HOCl in HepG2 cells at different time periods and discovered for the first time that 3-fluoro-10-hydroxyevodiamine, a potential anticancer molecule, generated HOCl. The **C7**-based detection system is unprecedented and offers a promising tool for evaluating ROS-generating anticancer drugs. More broadly, the study will pave the way to evaluate the interrelated roles of HOCl in various physiological and pathological conditions.

Conflicts of interest

The authors declare that they have no competing financial interests.

Acknowledgements

References

1 K. J. Barnham, C. L. Masters and A. I. Bush, *Nat. Rev. Drug Discovery*, 2004, **3**, 205–214.

2 T. Strowig, J. Henao-Mejia, E. Elinav and R. Flavell, *Nature*, 2012, **481**, 278–286.

3 M. P. Murphy, A. Holmgren, N. G. Larsson, B. Halliwell, C. J. Chang, B. Kalyanaraman, S. G. Rhee, P. J. Thornalley, L. Partridge, D. Gems, T. Nystrom, V. Belousov, P. T. Schumacker and C. C. Winterbourn, *Cell Metab.*, 2011, **13**, 361–366.

4 N. Branzk, A. Lubojemska, S. E. Hardison, Q. Wang, M. G. Gutierrez, G. D. Brown and V. Papayannopoulos, *Nat. Immunol.*, 2014, **15**, 1017–1025.

5 T. Finkel, M. Serrano and M. A. Blasco, *Nature*, 2007, **448**, 767–774.

6 H. J. Kwon, D. Kim, K. Seo, Y. G. Kim, S. I. Han, T. Kang, M. Soh and T. Hyeon, *Angew. Chem., Int. Ed.*, 2018, **57**, 9408–9412.

7 R. P. Wu, T. Hayashi, H. B. Cottam, G. Jin, S. Yao, C. C. Wu, M. D. Rosenbach, M. Corr, R. B. Schwab and D. A. Carson, *Proc. Natl. Acad. Sci. U. S. A.*, 2010, **107**, 7479–7484.

8 C. Nathan and A. Cunningham-Bussel, *Nat. Rev. Immunol.*, 2013, **13**, 349–361.

9 P. Pei, C. Sun, W. Tao, J. Li, X. Yang and J. Wang, *Biomaterials*, 2018, **188**, 74–82.

10 X. Xu, P. E. Saw, W. Tao, Y. Li, X. Ji, S. Bhasin, Y. Liu, D. Ayyash, J. Rasmussen, M. Huo, J. Shi and O. C. Farokhzad, *Adv. Mater.*, 2017, **29**, 1700141.

11 K. Mabuchi, H. Maki, T. Itaya, T. Suzuki, M. Nomoto, S. Sakaoka, A. Morikami, T. Higashiyama, Y. Tada, W. Busch and H. Tsukagoshi, *Proc. Natl. Acad. Sci. U. S. A.*, 2018, **115**, E4710–E4719.

12 N. Anicic, M. Vukomanovic, T. Koklic and D. Suvorov, *Small*, 2018, **14**, 1800205.

13 S. Rodic and M. D. Vincent, *Int. J. Cancer*, 2018, **142**, 440–448.

14 R. S. Balaban, S. Nemoto and T. Finkel, *Cell*, 2005, **120**, 483–495.

15 K. E. Broaders, S. Grandhe and J. M. Frechet, *J. Am. Chem. Soc.*, 2011, **133**, 756–758.

16 C. d. G. Lux, S. Joshi-Barr, T. Nguyen, E. Mahmoud, E. Schopf, N. Fomina and A. Almutairi, *J. Am. Chem. Soc.*, 2012, **134**, 15758–15764.

17 Y. Zou, D. Zhao, C. Yan, Y. Ji, J. Liu, J. Xu, Y. Lai, J. Tian, Y. Zhang and Z. Huang, *J. Med. Chem.*, 2018, **61**, 1821–1832.

18 L. Raj, T. Ide, A. U. Gurkar, M. Foley, M. Schenone, X. Li, N. J. Tolliday, T. R. Golub, S. A. Carr, A. F. Shamji, A. M. Stern, A. Mandinova, S. L. Schreiber and S. W. Lee, *Nature*, 2011, **475**, 231–234.

19 J. S. Bair, R. Palchaudhuri and P. J. Hergenrother, *J. Am. Chem. Soc.*, 2010, **132**, 5469–5478.

20 J. R. Kirshner, S. He, V. Balasubramanyam, J. Kepros, C. Y. Yang, M. Zhang, Z. Du, J. Barsoum and J. Bertin, *Mol. Cancer Ther.*, 2008, **7**, 2319–2327.

21 S. J. O'Day, A. M. Eggermont, V. Chiarion-Sileni, R. Kefford, J. J. Grob, L. Mortier, C. Robert, J. Schachter, A. Testori, J. Mackiewicz, P. Friedlander, C. Garbe, S. Ugurel, F. Collichio, W. Guo, J. Lufkin, S. Bahcall, V. Vukovic and A. Hauschild, *J. Clin. Oncol.*, 2013, **31**, 1211–1218.

22 R. K. Blackman, K. Cheung-Ong, M. Gebbia, D. A. Proia, S. He, J. Kepros, A. Jonneaux, P. Marchetti, J. Kluza, P. E. Rao, Y. Wada, G. Giaever and C. Nislow, *PLoS One*, 2012, **7**, e29798.

23 X. Liang, S. Xu, J. Zhang, J. Li and Q. Shen, *ACS Appl. Mater. Interfaces*, 2018, **10**, 38749–38759.

24 H. Zhu, J. Fan, J. Wang, H. Mu and X. Peng, *J. Am. Chem. Soc.*, 2014, **136**, 12820–12823.

25 J. Zielonka, J. Joseph, A. Sikora, M. Hardy, O. Ouari, J. Vasquez-Vivar, G. Cheng, M. Lopez and B. Kalyanaraman, *Chem. Rev.*, 2017, **117**, 10043–10120.

26 Y. Koide, Y. Urano, K. Hanaoka, T. Terai and T. Nagano, *J. Am. Chem. Soc.*, 2011, **133**, 5680–5682.

27 L. Yuan, W. Lin, Y. Yang and H. Chen, *J. Am. Chem. Soc.*, 2012, **134**, 1200–1211.

28 R. Zhang, J. Zhao, G. Han, Z. Liu, C. Liu, C. Zhang, B. Liu, C. Jiang, R. Liu, T. Zhao, M. Y. Han and Z. Zhang, *J. Am. Chem. Soc.*, 2016, **138**, 3769–3778.

29 L. Wu, I. C. Wu, C. C. DuFort, M. A. Carlson, X. Wu, L. Chen, C. T. Kuo, Y. Qin, J. Yu, S. R. Hingorani and D. T. Chiu, *J. Am. Chem. Soc.*, 2017, **139**, 6911–6918.

30 H. Ma, B. Song, Y. Wang, D. Cong, Y. Jiang and J. Yuan, *Chem. Sci.*, 2017, **8**, 150–159.

31 K. Dou, Q. Fu, G. Chen, F. Yu, Y. Liu, Z. Cao, G. Li, X. Zhao, L. Xia, L. Chen, H. Wang and J. You, *Biomaterials*, 2017, **133**, 82–93.

32 X. Jiao, Y. Xiao, Y. Li, M. Liang, X. Xie, X. Wang and B. Tang, *Anal. Chem.*, 2018, **90**, 7510–7516.

33 M. Ren, Z. Li, J. Nie, L. Wang and W. Lin, *Chem. Commun.*, 2018, **54**, 9238–9241.

34 C. Zhang, Q. Nie, I. Ismail, Z. Xi and L. Yi, *Chem. Commun.*, 2018, **54**, 3835–3838.

35 L. Yuan, L. Wang, B. K. Agrawalla, S. J. Park, H. Zhu, B. Sivaraman, J. Peng, Q. H. Xu and Y. T. Chang, *J. Am. Chem. Soc.*, 2015, **137**, 5930–5938.

36 P. Wei, W. Yuan, F. Xue, W. Zhou, R. Li, D. Zhang and T. Yi, *Chem. Sci.*, 2018, **9**, 495–501.

37 Y. L. Pak, S. J. Park, G. Song, Y. Yim, H. Kang, H. M. Kim, J. Bouffard and J. Yoon, *Anal. Chem.*, 2018, **90**, 12937–12943.

38 Q. Xu, C. Heo, J. A. Kim, H. S. Lee, Y. Hu, D. Kim, K. M. K. Swamy, G. Kim, S. J. Nam, H. M. Kim and J. Yoon, *Anal. Chem.*, 2016, **88**, 6615–6620.

39 Z. Mao, M. Ye, W. Hu, X. Ye, Y. Wang, H. Zhang, C. Li and Z. Liu, *Chem. Sci.*, 2018, **9**, 6035–6040.

40 A. C. Sedgwick, L. Wu, H. H. Han, S. D. Bull, X. P. He, T. D. James, J. L. Sessler, B. Z. Tang, H. Tian and J. Yoon, *Chem. Soc. Rev.*, 2018, **47**, 8842–8880.

41 H. Chen, Y. Tang, M. Ren and W. Lin, *Chem. Sci.*, 2016, **7**, 1896–1903.

42 L. Yuan, W. Lin, Y. Xie, B. Chen and S. Zhu, *J. Am. Chem. Soc.*, 2012, **134**, 1305–1315.

43 H. Komatsu, T. Miki, D. Citterio, T. Kubota, Y. Shindo, Y. Kitamura, K. Oka and K. Suzuki, *J. Am. Chem. Soc.*, 2005, **127**, 10798–10799.

44 B. Zhu, P. Li, W. Shu, X. Wang, C. Liu, Y. Wang, Z. Wang, Y. Wang and B. Tang, *Anal. Chem.*, 2016, **88**, 12532–12538.

45 Y. Jiang, G. Zheng, Q. Duan, L. Yang, J. Zhang, H. Zhang, J. He, H. Sun and D. Ho, *Chem. Commun.*, 2018, **54**, 7967–7970.

46 L. Wu, Q. Yang, L. Liu, A. C. Sedgwick, A. J. Cresswell, S. D. Bull, C. Huang and T. D. James, *Chem. Commun.*, 2018, **54**, 8522–8525.

47 P. Xing, Z. Zhang, Y. Niu, Y. Qi, L. Dong and C. Wang, *Chem. Commun.*, 2018, **54**, 9889–9892.

48 J. Sun and F. Feng, *Analyst*, 2018, **143**, 4251–4255.

49 H. Xiao, P. Li, X. Hu, X. Shi, W. Zhang and B. Tang, *Chem. Sci.*, 2016, **7**, 6153–6159.

50 J. Zielonka, J. Joseph, A. Sikora, M. Hardy, O. Ouari, J. Vasquez-Vivar, G. Cheng, M. Lopez and B. Kalyanaraman, *Chem. Rev.*, 2017, **117**, 10043–10120.

51 Y. Huang, G. Zhang, F. Hu, Y. Jin, R. Zhao and D. Zhang, *Chem. Sci.*, 2016, **7**, 7013–7019.

52 G. Dong, S. Wang, Z. Miao, J. Yao, Y. Zhang, Z. Guo, W. Zhang and C. Sheng, *J. Med. Chem.*, 2012, **55**, 7593–7613.